COMMUNICATION

Check for updates

Oxidative dissolution of lithium and manganese from lithium manganospinel (LiMn$_2$O$_4$): towards climate-smart processes for critical metal recycling†

Rhys A. Ward,*[ab] Dávid Kocsis*[abc] and Jay D. Wadhawan [iD] *[ab]

This work reports the oxidative breakdown of the LiMn$_2$O$_4$ structure using alkaline hypochlorite, as a method for recovering both lithium and manganese species. The heterogeneous dissolution rate for this process is monitored through the formation of the permanganate ion. It is found that reaction occurs under activation control, with a barrier that matches that for electron hopping within the spinel. Moreover, this activation barrier is smaller than those observed for typical conventional methods of recovery of lithium or manganese from LiMn$_2$O$_4$; accordingly, the new process is suggested to be climate-smart, despite the low, single-pass, recovery efficiency that results from slow surface kinetics.

The transition to the wide-scale deployment of renewable energy holds a plethora of challenges associated with technical, environmental, societal and governance aspects. Since this clean energy transition is mineral-intensive,[1,2] it requires a substantial material footprint, even though the overall amount of greenhouse gas emissions is lower than those associated with the use of fossil fuels.[1] Accordingly, many mineral commodities are labelled as "critical" – their economic importance and supply risk both exceed certain thresholds.[3–7] However, it is also recognised that supply risk to a particular country is extremely sensitive to the global market conditions, especially when there is little access to indigenous sources of specific minerals at economically viable grades.[8–10] For example, the USA is wholly reliant on imports for their manganese supply[11] – a key metal chiefly used as a deoxidiser and desulphuriser in steel manufacture,[12] and thus impacts on the infrastructure for low-carbon energy technologies (wind, hydroelectric, geothermal power).[1,2,4] The current instabilities in Eastern Europe, where Ukraine and Georgia typically contribute ca. 4% of world production (ore or concentrate) of manganese, but hold at least ca. 10% of identified world manganese reserves,[13] may cause economic stress in the global manganese supply.[14] Likewise, mineral flow analysis indicates that the EU and the UK (notwithstanding current explorations in South-West England[15]) obtain the majority of their lithium products, required for battery-based energy storage, from China.[16,17] This promotes the development of ambitious, industrial recycling programmes, particularly of lithium batteries,[18,19] where a number of routes have been proposed for lithium battery cathodes, including pyrometallurgical or hydrometallurgical recovery,[20] solvent extraction,[21] or electrochemical[22] and direct recycling.[23] However, environmentally responsible resource recovery and recycling encourages innovation in "climate-smart" pathways, which use lower amounts of energy and/or water than current practices.[1,24]

One way to achieve climate-smart "urban mining"[25] is through the development of chemical leaching processes that require a lower activation energy than alternatives. This requires knowledge of the dissolution kinetics and the identification as to whether leaching operates under activation or mass transfer control. This is important since, if limited by slow mass transfer, the stirring rate of mineral concentrates/powders in the lixiviant will enable faster dissolution; whereas, if the heterogeneous chemical reaction determines the rate of dissolution, the process can capitalise on faster dissolution rates at high temperatures, or smaller particle sizes (larger interfacial areas). It follows that monitoring the kinetics with temperature empowers the determination of the activation energy of the dissolution: this is typically ca. 8–17 kJ mol^{-1} for diffusion control, and greater than 42 kJ mol^{-1} for chemical control.[26]

In this communication, following our earlier work on the redox removal of iron and manganese impurities in slaked lime using alkaline hypochlorite,[27] we report a redox method for breaking down the framework of lithium managnospinel, LiMn$_2$O$_4$ – a material used as a lithium-ion battery cathode.[19,23] This enables the solubilisation of both lithium and manganese as

^{a} Department of Chemical Engineering, The University of Hull, Cottingham Road, Kingston-upon-Hull HU6 7RX, UK. E-mail: r.ward4@hull.ac.uk, dkocsis@singletonbirch.co.uk, j.wadhawan@hull.ac.uk

^{b} Aura Innovation Centre, Bridgehead Business Park, Meadow Road, Hessle HU13 0GD, UK

^{c} Singleton Birch, Ltd., Melton Ross Quarries, Barnetby, DN38 6AE, North Lincolnshire, UK

a pathway for total recovery, rather than merely recovery of one species, with the remainder being used for direct recycling. We focus on the initial dissolution kinetics, since our previous work has illustrated how such initial kinetics can be maintained in a "cascading" mineral processing flowsheet.[27] Moreover, this enables the unravelling of the activation energy required for the dissolution – for reactions under activation control, the lower this is, compared with conventional, reductive acidic leaching[28] of $LiMn_2O_4$, the more climate-smart the recovery process becomes, assuming all other variables (such as leaching time) remain constant.

Lithium manganospinel ($LiMn_2O_4$) has a normal spinel structure (space group $Fd\bar{3}m$) with a cubic close-packed oxide lattice, with manganese in the half of the octahedral positions, and lithium in an eighth of the tetrahedral holes.[29–33] The manganese is present as both Mn^{III} and Mn^{IV}, with the former species (high-spin d^4) undergoing a co-operative Jahn–Teller distortion, yielding a tetragonal elongation at low temperature, that is noticeable through a first-order phase change around ambient temperature,[32] and which also occurs on increasing lithiation.[29–31] In operation as a battery cathode,[33] since $LiMn_2O_4$ carries DC current through Mn^{III}/Mn^{IV} electron hopping,[31,32] the expansion and contraction in the lattice, through the Jahn–Teller distortion, can lead to stress-induced cracking, particularly at high current drain.[33] Furthermore, it is thought[34] that Mn^{III} disproportionates to Mn^{II} and Mn^{IV}, which gives rise to the well-known capacity-fade ("aging") of this battery material,[35] as the Mn^{II} species dissolves in the electrolyte.[36] This dissolution process is controlled by surface kinetics, and is faster for smaller particles.[37] It occurs with an activation energy of $ca.$ 70 kJ mol^{-1} (for $LiMn_2O_4$ dissolution into a 50:50 vol% solution of ethylene carbonate and dimethylene carbonate containing 1.0 M $LiPF_6$).[37] This activation energy is larger than that required for Mn^{2+} dissolution using SO_2 to reduce $MnOOH$ (16–65 kJ mol^{-1}) under ambient conditions,[38] but comparable with those required for dissolution from manganese oxides by sulfuric acid:[39] 68 ± 2 kJ mol^{-1} (MnO), 80 ± 2 kJ mol^{-1} (Mn_3O_4), 86 ± 2 kJ mol^{-1} (Mn_2O_3) and 90 ± 2 kJ mol^{-1} (MnO_2). It is noteworthy that LeBlanc and Fogler[40] observed that manganese dissolution from this oxide series using mineral haloacids is more rapid, as the overall manganese oxidation state is lowered, with MnO dissolution having sufficiently low activation energies ($ca.$ 18–20 kJ mol^{-1}) for the chemical dissolution to be mass-transfer controlled, with reductive dissolution of the higher oxidation states requiring activation energies of between $ca.$ 18–97 kJ mol^{-1}. Furthermore, for Mn_3O_4, the activation energy for manganese dissolution as MnO_4^- determined by our previous work using alkaline hypochlorite[27] is $ca.$ 40% smaller than that reported for sulfuric acid above. Given, the Pourbaix diagram for $LiMn_2O_4$ indicates[28] its stability above $ca.$ pH 12 (at 90 °C), this encourages the examination of the possibility of manganese (and therefore lithium) dissolution from $LiMn_2O_4$ under similar conditions.

Incubation of $LiMn_2O_4$ (325 mesh, corresponding to particles of diameter $ca.$ 44 μm) with alkaline hypochlorite (8%) at ambient temperature overnight furnished a pale pink supernatant, with a UV-visible absorption spectrum indicating the formation of permanganate (for experimental details, see the ESI,† ESI1). As discussed in ESI2 (ESI†), this is consistent with the following overall process, where de-lithiation occurs with the breakdown of the manganese oxide framework.

$$2LiMn_2O_4(s) + 7ClO^-(aq) + 2OH^-(aq)$$
$$\rightarrow 2Li^+(aq) + 4MnO_4^-(aq) + 7Cl^- + H_2O(l) \quad (A)$$
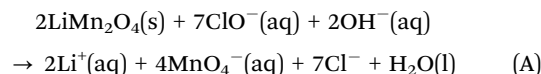
At pH 14, the standard electrode potential for the ClO^-/Cl^- redox couple is +0.89 V $vs.$ the standard hydrogen electrode (SHE).[41] The oxidative de-lithiation of $LiMn_2O_4$, (eqn (B)) has been reported to require similar potentials in lithium-based supporting electrolytes:[42–45]

$$LiMn_2O_4(s) \rightarrow xLi^+(aq) + xe^- + Li_{1-x}Mn_2O_4(s) \quad (B)$$
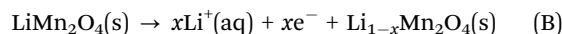
However, this reaction requires much higher potentials in sodium hydroxide electrolytes.[46] Accordingly, as indicated in ESI2 (ESI†), the following reaction sequence is likely to occur,

$$2LiMn_2O_4(s) + xClO^-(aq) + xH_2O(l)$$
$$\rightarrow 2Li_{1-x}Mn_2O_4(s) + 2xLi^+(aq) + xCl^- + 2xOH^-(aq)$$
$$(C)$$

$$Li_{1-x}Mn_2O_4(s) + \tfrac{1}{2}(5-x)ClO^-(aq) + (3+x)OH^-(aq)$$
$$\rightarrow (1-x)Li^+(aq) + 2MnO_4^{2-}(aq) + \tfrac{1}{2}(5-x)Cl^-(aq) + \tfrac{1}{2}(3+x)H_2O(l) \quad (D)$$

$$2MnO_4^{2-}(aq) + ClO^-(aq) + H_2O(l)$$
$$\rightarrow 2MnO_4^-(aq) + Cl^-(aq) + 2OH^-(aq) \quad (E)$$
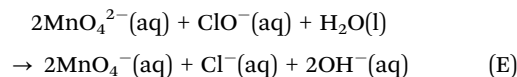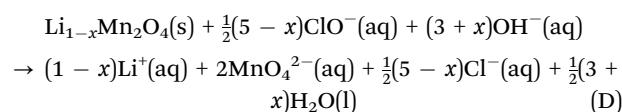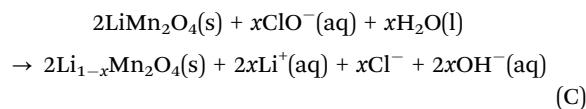
where the lithiated manganese dioxide species is likely to be the layered[30] Mn_2O_4 species of λ-MnO_2: this is known as the end-product from acidic de-lithiation.[34] This initial reaction sequence is further consistent with the ability of manganese dioxide to adsorb lithium ions in solution.[47] Since electron transfer kinetics across a semiconductor/electrolyte interface can be described through the normal Marcus region,[48] the slowest reactions are those with the smallest driving forces. As outlined in ESI2 (ESI†), it is likely that reaction (C) is the slowest chemical step. Note that thermodynamic considerations[49] suggest that, under the conditions employed (≤2% alkalinity, ≥8% available chlorine, corresponding to $ca.$0.625 M NaOH and ∼3 M NaClO), oxidation by dissolved oxygen is not significant.

As mentioned earlier, whilst the dissolution of most manganese oxides typically occurs under the control of surface kinetics, this is not always the case.[40] For surface redox reaction-controlled dissolution, a simple cubic law is typically followed.[50–53] However, the dissolution rate of irreversible chemical reactions occurring under mixed control by mass transfer and surface kinetics is given by:

$$Rate = \frac{k_{mt}k_{het}}{k_{mt}+k_{het}}c_{ClO^-}^{bulk} \quad (1)$$

in which k_{mt} is the mass transfer coefficient, k_{het} is the surface reaction rate constant and the bulk concentration of the hypochlorite lixiviant is $c_{ClO^-}^{bulk}$, and is formally derived in ESI3 (ESI†). In eqn (1), both mass transfer and rate coefficients have units

of length per unit time, so that the dissolution rate is equivalent to the flux (amount per unit time per unit area). The area involved is the interfacial area, and can be estimated through the total geometrical area of the particles (S). Assuming monodisperse spherical particles of radius r_0 (22 μm), we may approximate the total geometrical area as being the area of a single particle multiplied by the number of particles present. The latter is the ratio of the volume of the particles used to that corresponding to a single sphere, where the former is given by the mass of particles used (m_0) normalised by the bulk density of LiMn$_2$O$_4$ (ρ = 4.29 g cm^{-3}).[54] Thus,

$$S = \frac{3m_0}{r_0\rho} \qquad (2)$$

If the mass transport coefficient, k_{mt}, can be estimated, the heterogeneous reaction rate constant can be determined through monitoring the permanganate concentration change in the solution.

Accordingly, oxidative leaching experiments were undertaken through refluxing 80 mL of alkaline hypochlorite ($\leq$2% alkalinity, $\geq$8% available chlorine), with a fixed mass of LiMn$_2$O$_4$ (m_0 = 0.1 g or 1.0 g) at a known temperature, T, in the range 50 < T/°C < 100, for a constant time period (1 h), see ESI1 (ESI†). Our previous work,[27] suggests that this time period is sufficient for the initial rate to be monitored. Fig. 1 illustrates spectrophotometric analysis of an aliquot of the reaction solution taken after 60 min. It is clear that in all cases, MnO$_4^-$ is present, at concentrations in the range 30–170 μM, based on Beer–Lambert analysis through comparison with external MnO$_4^-$ calibration (λ_{max} = 525 nm; ε = 2085 L mol^{-1} cm^{-1}) over the range 25–560 μM.

The rate of LiMn$_2$O$_4$ dissolution is then given by,

$$\text{Rate} = \frac{1}{2} \frac{\text{Number of MnO}_4^- \text{ produced in time } \tau}{S} \qquad (3)$$

where the factor of $\frac{1}{2}$ results from the 1:2 stoichiometry of LiMn$_2$O$_4$: MnO$_4^-$ in eqn (A). Thus, combining eqn (1)–(3) affords:

$$k_{het} = \frac{k_{mt}k_{MnO_4^-}^{bulk} V_{sol}r_0\rho}{6k_{mt}\tau m_0 c_{ClO^-}^{bulk} - c_{MnO_4^-}^{bulk} V_{sol}r_0\rho} \qquad (4)$$

in which V_{sol} is the volume of alkaline hypochlorite used (80 mL).

As demonstrated in ESI4 (ESI†), the mass transfer coefficient (k_{mt}) is on the order of 10^{-4} m s^{-1} and demonstrates temperature dependence with activation energy of *ca.* 16 kJ mol^{-1}. In contrast, the mixed activation/mass transfer constant in eqn (1) is on the order of 10^{-11} m s^{-1}, which is substantially smaller than the mass transfer coefficient. This dissolutive flux thus corresponds to pure kinetics, with no contribution from mass transfer.[55] Accordingly, using eqn (4), the heterogeneous rate constant for the dissolution can be estimated. This is presented in Fig. 2, in the form of an Arrhenius plot. It is clear that in the temperature range studied, the true surface chemical rate constant (k_{het}) is independent of the starting mass of LiMn$_2$O$_4$.

Moreover, the rate constant increases with temperature, as expected; this dependency enables the estimation of the activation energy for the oxidative dissolution of 22 kJ mol^{-1} (0.23 eV). This is significantly smaller than required by other treatments,[36,38,40] and is for slow activation kinetics and not mass transfer in solution. Since the activation energy for electronic conductivity in LiMn$_2$O$_4$ semiconductors through electron hopping (small polaron) between Mn^{III} and Mn^{IV} sites has been given as between[56–58] 0.16–0.34 eV, this indicates that it is transport within the solid of Mn^{III} to the surface that rate limits the dissolution. This is consistent with reaction (C) being the slow step.


Fig. 1 Visible absorption spectrum of the permanganate product obtained from 1.0 g (red, blue and yellow) or 0.1 g (green) LiMn$_2$O$_4$ heated with 80 mL of alkaline hypochlorite solution after one hour at 54 °C (yellow), 72 °C (blue) or 95 °C (red and green).
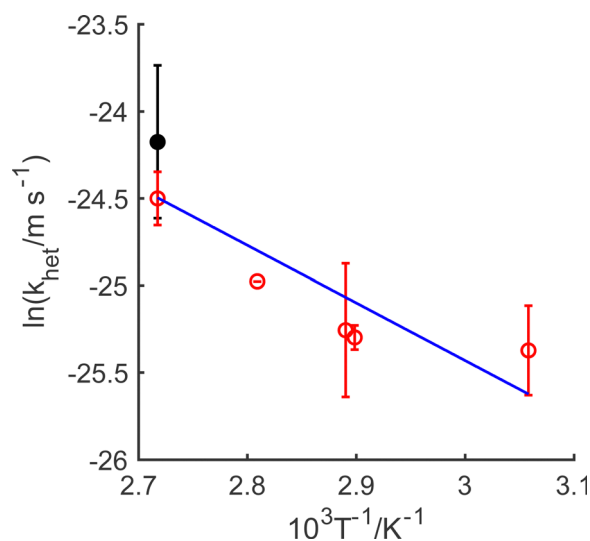

Fig. 2 Arrhenius plots illustrating the temperature dependence of the rate constant for oxidative dissolution. Open red circles correspond to 1.0 g LiMn$_2$O$_4$; closed black circles correspond to 0.1 g LiMn$_2$O$_4$. Mean data plotted, with maximum and minimum limits given through the error bars for measurements made in duplicate.

The activation energy for the oxidative, surface-controlled leaching of $LiMn_2O_4$ is lower than that reported for the surface kinetics-limited reductive leaching (activation energy of ~ 50 kJ mol^{-1}) $LiCoO_2$.[59] Both materials are semiconductors at ambient temperature: $LiMn_2O_4$ is an n-type semiconductor (band gap of 1.99 eV),[58] whilst, $LiCoO_2$ undergoes a semiconductor-to-metallic transition as lithium de-intercalation occurs.[60] When a metal is immersed into a redox electrolyte, equilibration of the Fermi level of the metal with that of the redox electrolyte occurs, and heterogeneous electron transfer is dominated by the continuum of electronic energy states in the electrode, where the density of states (the number of states per atom per unit energy) is assumed to be independent of energy, and for which the Fermi–Dirac distribution governs the occupancy probability of a given electronic energy state.[61] For oxidative leaching (corrosion) of metals, reduction of the chemical oxidant is an iso-energetic electron transfer into an unoccupied energy state in the solution species. This can occur from any occupied state within the electrode into the (assumed) Gaussian density of states function for the aqueous redox species. In contrast, when a semiconductor is in electronic contact with a redox electrolyte, charge can flow across the interface, which leads to the development of a space-charge region in the semiconductor, in which the band edges are pinned relative to the Fermi level of the solution phase species (assuming the semiconductor is defect-free).[61] In the case of $LiMn_2O_4$, the space-charge region has been reported to have a width of 44 nm.[58] Such band bending phenomena changes the concentrations of electrons and holes at the semiconductor side of the interface, and thus, hole (or electron) transfer can only occur through a narrow distribution of energies within the band continuum, whenever electronic overlap of semiconductor states with the solution Fermi energy occurs. As noted by LeBlanc and Folger,[40] the difference between the solution redox couple and the semiconductor band edge can be considered as the activation barrier for the heterogeneous redox process. Under standard conditions, the experimental solution at *ca.* pH 14 indicates that the valence band edge of $LiMn_2O_4$ has a value of *ca.* 0.78 V *vs.* SHE,[58] the oxidation process is predicted to be under activation control, as observed experimentally.

The manganese leaching efficiency (χ) is calculated from the ratio of the amount of manganese dissolved in solution as permanganate to the amount of manganese in the initial solid powder:[28]

$$\chi = \frac{c_{MnO_4^-}^{bulk} V_{sol}}{2 \times \frac{m_0}{181}} \times 100 \qquad (5)$$

where m_0 is the mass (in g) of $LiMnO_2$ (molar mass 181 g mol^{-1}) used initially. The data illustrated in Fig. 3 demonstrate that only slight leaching (0.2% maximum) occurs over the 60 min period using alkaline hypochlorite. Again, it is evident that there is little difference in the data for the different solid/water ratios used (1.25 g L^{-1} to 12.5 g L^{-1}). Moreover, the leaching rate is commensurate with those reported for the alternative oxidants of peroxydisulphate and bromine,[62] for which it is reported that lithium ion extraction occurs with only a slight dissolution of manganese.[62]
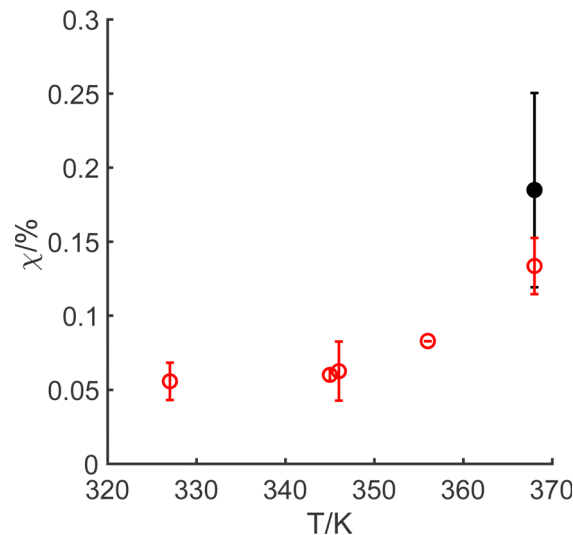

Fig. 3 Temperature dependence of the manganese leaching efficiency through oxidative dissolution with alkaline permanganate. Open red circles correspond to 1.0 g $LiMn_2O_4$; closed black circles correspond to 0.1 g $LiMn_2O_4$. Mean data plotted, with maximum and minimum limits given through the error bars for measurements made in duplicate.

In summary, the alternative oxidative leaching method illustrated in this work requires lower energy expenditure than current methods, owing to the smaller activation energy for the chemical reaction. Whilst only *ca.* 0.15% of the available manganese has been demonstrated to have dissolved through oxidation under the short time period, this is a climate-smart process. Although we have only studied a small range of solid/water levels (1.25 g L^{-1} to 12.5 g L^{-1}), since the chemistry is under pure kinetic control by the heterogeneous electron transfer, there is no dependence on the mass of the solid. This suggests that optimisation of this chemistry is possible, and this may enable a reduction in the water stress required for lithium and manganese recovery from $LiMn_2O_4$, although the 7 F mol^{-1} required by the overall reaction, reaction (A), indicates a compromise is necessary as hypochlorite is needed for both the initial and subsequent steps. The chemical system enables dissolution of the manganese framework,[62] and therefore allows both lithium ions and permanganate ions to be based in the solution. These two ions are readily separated in subsequent steps, since MnO_4^- is highly redox-active and can be reduced to MnO_2 by, for example, abating a reduced gas species (such as H_2S, SO_2, NO_2, *etc.*) at an appropriate pH, during industrial symbiotic chemical processes. In line with previous work,[27] in taking this forward, a cascading leaching process will need to be developed, to overcome the thermal decomposition of hypochlorite,[63] in order enable optimisation of the process conditions.

Conflicts of interest

There are no competing pecuniary interests to declare.

Acknowledgements

Notes and references

1 K. Hund, D. La Porta, T. P. Fabregas, T. Laing and J. Drexhage, *Minerals for Climate Action: The Mineral Intensity of the Clean Energy Transition*, World Bank, Washington, DC, 2020.

2 International Energy Agency, *The Role of Critical Minerals in Clean Energy Transitions*, IEA, Paris, 2021.

3 G. Gun, ed., *Critical Metals Handbook*, Wiley, Chichester, 2014.

4 National Research Council, *Minerals, Critical Minerals, and the US Economy*, The National Academies Press, Washington DC, 2008.

5 L. Simandl, G. J. Simandl and S. Paradis, Economic geology models V: speciality, critical, battery, magnet and photovoltaic materials – market, facts, projections and implications for exploration and development, *Geosci. Canada*, 2021, **48**, 73.

6 R. Pell, L. Tijsseling, K. Goodenough, F. Wall, Q. Dehaine, A. Grant, D. Deak, X. Yan and P. Whattoff, Towards sustainable extraction of technology materials through integrated approaches, *Nat. Rev. Earth Environ.*, 2021, **2**, 665.

7 R. Harrington, Mining our green future, *Nat. Rev. Mater.*, 2021, **6**, 456.

8 N. T. Nassar, J. Brainard, A. Gulley, R. Manley, G. Matos, G. Lederer, L. R. Bird, D. Pineault, E. Alonso, J. Gambogi and S. M. Fortier, Evaluating the mineral commodity supply risk of the U.S. manufacturing sector, *Sci. Adv.*, 2020, **6**, eaay8647.

9 B. K. Sovacol, S. H. Ali, M. Bazilian, B. Radley, B. Nemery, J. Okatz and D. Mulvaney, Sustainable minerals and metals for a low-carbon future: policy co-ordination is needed for global supply chains, *Science*, 2020, **367**, 30.

10 See, for example: D. Schrijvers, A. Hool, G. A. Blengini, W.-Q. Chen, J. Dewulf, R. Eggert, L. van Ellen, R. Gauss, J. Goddin, K. Habib, C. Hagelüken, A. Hirohata, M. Hofmann-Amtenbrink, J. Kosmol, M. Le Gleuher, M. Grohol, A. Ku, M.-H. Lee, G. Liu, K. Nansai, P. Nuss, D. Peck, A. Reller, G. Sonnemann, L. Tercero, A. Thorenz and P. A. Wäger, A review of methods and data to determine raw material criticality, *Resour., Conserv. Recycl.*, 2020, **155**, 104617.

11 K. J. Schulz, J. H. DeYoung Jr., R. R. Seal II and D. C. Bradley, ed., *Critical Mineral Resources of the United States: Economic and Environmental Geology and Prospects for Future Supply*, U. S. Geological Survey Professional Paper 1802, U. S. Geological Survey, Reston, Virginia, 2017.

12 See, for example: A. Street and W. Alexander, *Metals in the Service of Man*, Penguin Books, London, 11th edn, 1998.

13 Estimates based on data provided in U.S. Geological Survey, Mineral Commodity Summaries 2022, U.S. Geological Survey, Reston, Virginia, 2022.

14 This has been seen recently for the nickel market: following "unprecedented overnight increases in the three month nickel price...owing to the "evolving situation in Russia and Ukraine," the London Metal Exchange suspended nickel trading on March 8, 2022, with a number of subsequent trading updates in the light of price disruption events given since then, q.v. https://www.lme.com/en/metals/non-ferrous/lme-nickel (accessed March 30, 2022).

15 Two companies, British Lithium, Ltd. (https://british lithium.co.uk, accessed March 13, 2022) and Cornish Lithium (https://cornishlithium.com, accessed March 13, 2022) have been exploring the extraction of lithium from granite-based pegmatites and geothermal brine. For an overview of availability of lithium resources in the UK, see British Geological Survey, Raw Materials for Decarbonisation: The Potential for Lithium in the UK, British Geological Survey, Keyworth, 2020.

16 X. Sun, H. Hao, F. Zhao and Z. Liu, Tracing global lithium flow: a trade-linked material flow analysis, *Resour., Conserv. Recycl.*, 2017, **124**, 50.

17 E. Petavratzi and P. Josso, Global Material Flows of Lithium for the Lithium-Ion and Lithium Iron Phosphate Battery Markets, British Geological Survey Open Report, OR/21/055.

18 P. Meshram, B. D. Pandey and T. R. Mankhand, Extraction of lithium from primary and secondary sources by pre-treatment, leaching and separation: a comprehensive review, *Hydrometallurgy*, 2014, **150**, 192.

19 See, for example: L. Li, V. G. Deshmane, M. P. Paranthaman, R. Bhave, B. A. Moyer and S. Harrison, Lithium recovery from aqueous resources and batteries: a brief review, *Johnson Matthey Technol. Rev.*, 2018, **62**, 161.

20 L. Brückner, J. Frank and T. Elwert, Industrial recycling of lithium-ion batteries: a critical review of metallurgical process route, *Metals*, 2020, **10**, 1107.

21 T. H. Nguyen and M. S. Lee, A review on the separation of lithium ion from leach liquors of primary and secondary resources by solvent extraction with commercial extractants, *Processes*, 2018, **6**, 55.

22 See, for example: M. J. Lain, Recycling of lithium cells and batteries, *J. Power Sources*, 2001, **97–98**, 736.

23 G. Harper, R. Sommerville, E. Kendrick, L. Driscoll, P. Slater, R. Stolkin, A. Walton, P. Christensen, O. Heidrich, S. Lambert, A. Abbott, K. Ryder, L. Gaines and P. Anderson, Recycling lithium-ion batteries from electric vehicles, *Nature*, 2019, **575**, 75.

24 Water-stress is increasingly becoming an important consideration for the mining industry – see, for example: M. B. Revuelta, Whilst the water footprint of critical metal recycling facilities is not yet catalogued, it is important to design recovery processes that minimise water use, *Mineral Resources: From Exploration to Sustainability Assessment*, Springer Nature, Cham, 2018.

25 See, for example: C. Hageluken, Recycling of (critical) metals, in G. Gunn, ed., *Critical Metals Handbook*, Wiley, Chichester, 2014, p. 41.

26 See, for example: K. N. Han and M. C. Fuerstenau, Hydrometallurgy and solution kinetics, in M. C. Fuerstenau and K. N. Han, ed., *Principles of Mineral Processing*, Society for

Mining, Metallurgy and Exploration, Englewood, Colorado, 2003, p. 413.

27 D. Kocsis, R. A. Ward, C. R. Meyer, M. Thompson, T. J. Prior, S. M. Kelly, N. S. Lawrence and J. D. Wadhawan, Empowering clean water whilst safeguarding water distribution pipeline integrity: towards manganese- and iron-free lime hydrate for water treatment, *Environ. Sci.: Water Res. Technol.*, 2023, **9**, 833.

28 See, for example: Z. Li, L. He, Z. Wei Zhao, D. Wang and W. Xu, Recovery of lithium and manganese from scrap $LiMn_2O_4$ by slurry electrolysis, *ACS Sustainable Chem. Eng.*, 2019, 7, 16738.

29 M. M. Thackeray, W. I. F. David, P. G. Bruce and J. B. Goodenough, Lithium insertion into manganese spinels, *Mater. Res. Bull.*, 1983, **18**, 461.

30 M. M. Thackeray, Structural considerations of layered and spinel lithiated oxides for lithium-ion batteries, *J. Electrochem. Soc.*, 1995, **142**, 2558.

31 H. Berg, K. Goransson, B. Nolang and J. O. Thomas, Electronic structure and stability of the $Li_xMn_2O_4$ ($0 < x < 2$) system, *J. Mater. Chem.*, 1999, **9**, 2813.

32 S. Chitra, P. Kalyani, T. Mohan, M. Massot, S. Ziolkiewicz, R. Gangandharan, M. Eddrief and C. Julien, Physical properties of $LiMn_2O_4$ spinel prepared at moderate temperature, *Ionics*, 1998, **4**, 8.

33 T. Liu, A. Dai, J. Lu, Y. Yuan, Y. Xiao, L. Yu, M. Li, J. Gim, L. Ma, J. Liu, C. Zhan, L. Li, J. Zheng, Y. Ren, T. Wu, R. Shahbazian-Yasser, J. Wen, F. Pan and K. Amine, Correlation between manganese dissolution and dynamic phase stability in spinel-based lithium-ion battery, *Nat. Commun.*, 2019, **10**, 4721.

34 J. C. Hunter, Preparation of a new crystal form of manganese dioxide: λ-MnO_2, *J. Solid State Chem.*, 1981, **39**, 142.

35 D. Larcher, P. Courjal, R. H. Urbina, B. Gerand, A. Blyr, A. du Pasquier and J.-M. Tarascon, Synthesis of MnO_2 phases from $LiMn_2O_4$ in aqueous acidic media: mechanisms of phase transformations, reactivity and effects of Bi species, *J. Electrochem. Soc.*, 1998, **145**, 3392.

36 Y. Tesfamhret, H. Liu, Z. Chai, E. Berg and R. Younesi, On the manganese dissolution process from $LiMn_2O_4$ cathode materials, *ChemElectroChem*, 2021, **8**, 1516.

37 C. Lu and S. Lin, Dissolution kinetics of spinel lithium manganite and its relation to capacity fading in lithium-ion batteries, *J. Mater. Res.*, 2002, **17**, 1476.

38 W. Zhang and C. Y. Cheng, Manganese metallurgy review part 1: leaching of ores/secondary materials and recovery of electrolytic/chemical manganese dioxide, *Hydrometallurgy*, 2007, **89**, 137.

39 E. B. Godunov, A. D. Izotov and I. G. Gorichev, Dissolution of manganese oxides of various compositions in sulfuric acid solutions studied by kinetic methods, *Inorg. Mater.*, 2018, **54**, 66.

40 B. S. E. LeBlanc and H. S. Fogler, The role of conduction/valence bands and redox potential in accelerated mineral dissolution, *AIChE J.*, 1986, **32**, 1702.

41 W. M. Latimer, *The Oxidation States of the Elements and their Potentials in Aqueous Solution*, Prentice-Hall, New York, 2nd edn, 1952.

42 B. Tao, L. C. Yule, E. Daviddi, C. L. Bentley and P. R. Unwin, Correlative electrochemical microscopy of Li-ion (de)intercalation at a series of individual $LiMn_2O_4$ particles, *Angew. Chem., Int. Ed.*, 2019, **58**, 4606.

43 L. Köhler, M. E. Abrishami, V. Roddatis, J. Geppert and M. Risch, Mechanistic parameters of electrocatalytic water oxidation on $LiMn_2O_4$ in comparison to natural photosynthesis, *ChemSusChem*, 2017, **10**, 4479.

44 T. Ohzuku, M. Kitagawa and T. Hirai, Electrochemistry of manganese dioxide in lithium non-aqueous cell III: X-ray diffractional study on the reduction of spinel-related manganese dioxide, *J. Electrochem. Soc.*, 1990, **137**, 769.

45 E. Hosono, T. Kudo, I. Honma, H. Matsuda and H. Zhou, Synthesis of single crystalline spinel $LiMn_2O_4$ nanowires for a lithium-ion battery with high power density, *Nano Lett.*, 2009, **9**, 1045.

46 M. Baumung, L. Kollenbach, L. Xi and M. Risch, Undesired bulk oxidation of $LiMn_2O_4$ increases overpotential of electrocatalytic water oxidation in lithium hydroxide electrolytes, *ChemSusChem*, 2019, **20**, 2981.

47 S. K. Ghosh, Diversity in the family of manganese oxides at the nanoscale: from fundamentals to applications, *ACS Omega*, 2020, **5**, 25493.

48 B. Gilbert and G. A. Waychunas, The timescale of mineral redox reactions, in I. A. M. Ahmed and K. A. Hudson-Edwards, ed., *Redox-Reactive Minerals: Properties, Reactions and Applications in Natural Systems and Clean Technologies, EMU Notes in Mineralogy*, The Mineralogical Society of Great Britain and Ireland, London, 2017, ch. 4, vol. 17, p. 55.

49 T. A. Zordan and L. G. Hepler, Thermochemistry and oxidation potentials of manganese and its compounds, *Chem. Rev.*, 1968, **68**, 737.

50 M. G. Segal and R. M. Sellers, Reactions of solid iron(III) oxides with aqueous reducing agents, *J. Chem. Soc., Chem. Commun.*, 1980, 991.

51 A. Mills and D. Worsley, Kinetics of redox dissolution of soft-centre particles, *J. Chem. Soc., Faraday Trans.*, 1990, **86**, 3405.

52 J. D. Wadhawan, R. G. Evans, C. E. Banks, S. J. Wilkins, R. R. France, N. J. Oldham, A. J. Fairbanks, B. Wood, D. J. Walton, U. Schroder and R. G. Compton, Voltammetry of electroactive oil droplets: electrochemically induced ion insertion, expulsion and reaction processes at microdroplets of N,N,N',N'-tetraalkyl-para-phenylenediamine (TRPD, R = n-butyl, n-hexyl, n-heptyl, n-nonyl), *J. Phys. Chem.*, 2002, **106**, 9619.

53 C. L. Forryan, O. V. Klymenko, C. M. Brennan and R. G. Compton, Reactions at the solid-liquid interface: surface-controlled dissolution of solid particles: the dissolution of potassium bicarbonate in dimethylformamide, *J. Phys. Chem. B*, 2005, **109**, 2862.

54 Bulk crystalline density of LiMn2O4 is reported at the following URL. **https://materials.springer.com/isp/crystallographic/docs/sd_1628205** (accessed March 15, 2022).

55 See, for example: J. H. Atherton, Mechanism in two-phase reaction systems: coupled mass transfer and chemical reaction, in R. G. Compton and G. Hancock, ed., *Research in Chemical Kinetics*, Elsevier, Amsterdam, 1994, vol. 2, p. 193.

56 S. Chitra, P. Kalyani, T. Mohan, M. Massot, S. Ziolkiewicz, R. Gangandharan, M. Eddriel and C. Julien, Physical properties of $LiMn_2O_4$ spinel prepared at moderate temperature, *Ionics*, 1998, **4**, 8.

57 E. Iguchi, Y. Tokuda, H. Nakatsugawa and F. Munakata, Electrical transport properties in $LiMn_2O_4$, $Li_{0.95}Mn_2O_4$ and $LiMn_{1.95}B_{0.05}O_4$ (B = Al or Ga) around room temperature, *J. Appl. Phys.*, 2002, **91**, 2149.

58 S. Douafer, H. Lahmar, M. Benamira, G. Rekhila and M. Trari, Physical and photoelectrochemical properties of the spinel $LiMn_2O_4$ and its application in photocatalysis, *J. Phys. Chem. Solids*, 2018, **118**, 62.

59 C. K. Lee and K.-I. Rhee, Reductive leaching of cathodic active materials from lithium-ion battery wastes, *Hydrometallurgy*, 2003, **68**, 5.

60 See, for example: H. Kang, J. Lee, T. Rodgers, J.-H. Shim and S. Lee, Electrical conductivity of de-lithiated lithium cobalt oxides: conductive atomic force microscopy and density functional theory study, *J. Phys. Chem. C*, 2019, **123**, 17703.

61 See, for example: H. Gerischer, Charge transfer processes at semiconductor-electrolyte interfaces in connection with problems of catalysis, *Surf. Sci.*, 1969, **18**, 97.

62 This type of approach for lithium-ion recovery has already been used before – see: K. Ooi, Y. Miyai, S. Kathoh, H. Maeda and M. Abe, Lithium-ion insertion/extraction with λ-MnO_2 in the aqueous phase, *Chem. Lett.*, 1988, 989.

63 L. C. Adam and G. Gordon, Hypochlorite ion decomposition: effects of temperature, ionic strength, and chloride ion, *Inorg. Chem.*, 1999, **38**, 1299.